Experiences with Sub-Arctic Sensor Network Deployment and Feasibility of Geothermal Energy Harvesting

Priyesh Pappinisseri Puluckul
Maarten Weyn
IDLab—Faculty of Applied Engineering, University of Antwerp—imec
Antwerp, Belgium
priyesh.pappinisseripuluckul@uantwerpen.be
maarten.weyn@uantwerpen.be

ABSTRACT

This paper discusses the experiences gained from designing, deploying and maintaining low-power wireless sensor networks in three geothermally active remote locations in Iceland. The purpose of deploying the network was to collect soil temperature data and investigate the impact of global warming on (sub)Arctic climate and subsequent carbon release. Functional networks from three sites with no direct access to power and the internet have been providing researchers with insight into the warming impacts since 2021. The network employs low-power wireless sensor nodes equipped with DASH7 communication protocol, providing real-time data and remote access to sensors and instruments deployed in the field. In addition to discussing the architecture and deployment of the network, we conduct a primary analysis using models and methods to demonstrate the feasibility of harvesting energy from the temperature gradient between geothermally active soil and air.

CCS CONCEPTS

• Computer systems organization \rightarrow Embedded and cyber-physical systems; Embedded systems; Sensor networks; Embedded hardware:

KEYWORDS

Wireless Sensor Networks, Energy Harvesting, Geothermal Energy, Field Deployment, DASH7

ACM Reference Format:

1 INTRODUCTION

The Arctic ecosystem is a large reservoir of carbon, developed over millions of years. Climate changes and subsequent global warming cause the ecosystem to release a considerable amount of stored

Permission to make digital or hard copies of all or part of this work for personal or classroom use is granted without fee provided that copies are not made or distributed for profit or commercial advantage and that copies bear this notice and the full citation on the first page. Copyrights for components of this work owned by others than the author(s) must be honored. Abstracting with credit is permitted. To copy otherwise, or republish, to post on servers or to redistribute to lists, requires prior specific permission and/or a fee. Request permissions from permissions@acm.org.

Conference acronym 'XX, June 03-05, 2018, Woodstock, NY

© 2024 Copyright held by the owner/author(s). Publication rights licensed to ACM. ACM ISBN 978-1-4503-XXXX-X/18/06 https://doi.org/XXXXXXXXXXXXXXX

carbon, significantly impacting the carbon cycle. It is estimated that close to 30% of the global carbon is stored in northern high latitude regions, despite it covering only 5% global soil surface [7]. Therefore, understanding the future release of carbon from the Arctic system and its impact on climate is crucial. However, estimating the effect of future warming requires soil temperature manipulating experiments that are often costly and not scalable. In this regard, the ForHot site located in the village of Hveragerði in southern Iceland [2] offers a geothermally controlled soil temperature which can be used as a large-scale controlled environment to study the impact of global warming and future carbon release. Exploiting this natural laboratory and utilizing the technological advancements in Internet of Things (IoT) and Machine Learning (ML), an interdisciplinary research program was established, in an attempt to investigate the response of the sub(Arctic) ecosystem to climate changes and the release of carbon. Therefore, it was the motivation for this research to deploy low-power Wireless Sensor Networks (WSNs) for long-term monitoring of soil temperature from these





Figure 1: Deployment at one of the geothermally warmed sites at the ForHot site in Iceland.

The primary requirements of the project are:

- deploy low-power wireless sensor nodes to collect data: soil temperature sensor, soil water content sensor and weather station.
- to provide access to the wireless sensor nodes over a remote interface so that, parameters of the sensors such as sampling rate and sensor type can be configured over the air if required.

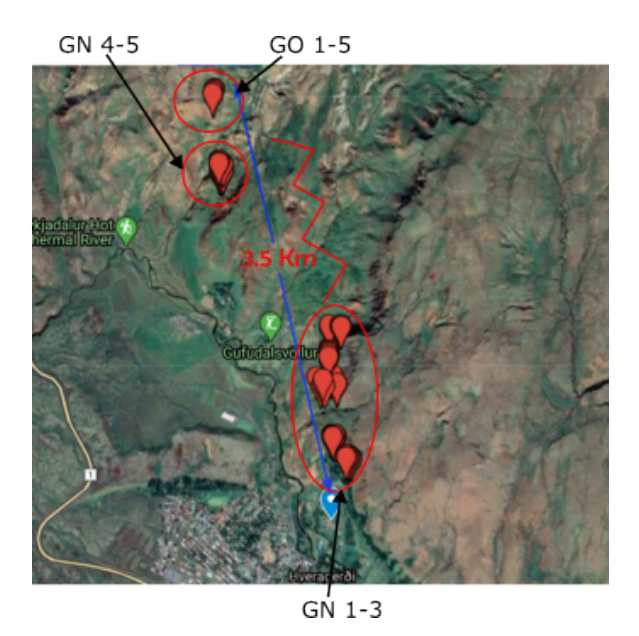


Figure 2: Google earth map showing the three sites are ForHot.

- to provide real-time ground truth to drone-based remote soil temperature sensing methods. This allows drones to collect the ground truth and remote sensing data simultaneously and cross-verify the estimations.
- Enable modular architecture and seamless sensor interface.
- Ensure a long-term operation; at least 3 years or more.

1.1 Deployment Sites

The ForHot site is divided into different sections based on the nature of heating and location as Forest New (FN), Grassland New (GN) and Grassland Old (GO) [8]. The soil at the GO site has been warmed since 1963. Whereas, the warming at FN and GN started only after the massive earthquake in 2008 which affected the nearby geothermal systems and consequently started the warming process. The FN site is characterised by the presence of spruce trees and GO and GN are mostly grass. Moreover, all the sites are characterised by tough terrains and steep hills dispersed over a wide area as shown in Fig. 2. Each site is divided into 5 (FN/GN/GO 1-5) plots and each plot is further divided into 6 transects (A-F) of 50 cm x 50 cm size. These transects are classified based on the warming level; transect A is unwarmed, i.e. mean annual temperature is approximately 0 °C, B is warmed by 1 °C, C by 3 °C, D by 5 °C and F by 10 °C. All the plots in GO are situated in nearby points whereas those in GN are scattered (GN 1-3 and GN 4-5) at different locations as shown in Fig. 2. The plots are GO, GN 1-3 and GN 4-5 are considered for deployment. The sensors are required to measure soil temperature in each transect at 10 cm depth, soil water content in at least one of the transects and a weather station for the sites.

2 NETWORK COMPONENTS AND DESIGN

This section presents the architecture of the overall network and the hardware-software design of different network components.

2.1 Choices of Wireless Communication

We considered three possible Low Power Wide Area Network (LP-WAN) standards at the initial stage of design- LoRaWAN, NB-IoT and DASH7. LoRaWAN can provide long-range connectivity at low data rates with extremely low power consumption. NB-IoT, on the other hand, co-exists with cellular networks and can enable a wide range of connectivity. However, NB-IoT has a relatively higher power consumption than LoRaWAN devices [5]. DASH7 is another communication protocol for low power IoT in the ISM band [11]. DASH7 can enable connectivity over 2 km in outdoor conditions and has comparable power consumption levels with LoRaWAN. Therefore, they are not truly LPWAN technology but a mid-range connectivity option.

When the FutureArctic deployment was planned, no NB-IoT network was established in Iceland. Consequently, NB-IoT was excluded from further discussions. An advantage of LoRaWAN over DASH7 is its long range. Whereas, DASH7 has the advantage of low-power wake-ups which is important for establishing downlink communication to the devices. Though LoRaWAN supports downlink transmission, they are either bound to up-link transmissions (Class A) or require strict synchronization (Class B). DASH7, on the other hand, requires no periodic synchronization to enable downlink transmission.

DASH7 Alliance Protocol (D7A) is a bidirectional ISM band protocol for low-power wireless sensor and actuator networks. DASH7 standard is derived from the ISO/IEC 18000-7 which specifies standards for active RFIDs. With its medium-range capabilities, DASH7 fills the gap between short and long-range communication protocols for low-power devices. The physical layer of DASH uses GFSK modulation with the MAC layer using CSMA-CA for collision avoidance. The network layer of DASH7 defines D7A Advertising Protocol (D7AAdvP) which handles the ad-hoc synchronization of the devices. The ad-hoc synchronization enables low-power downlink transmission to end devices. At the application layer, DASH7 defines the Application Layer Programming (ALP) which handles the application layer-related transactions. The application layer of the DASH7 is tailored to work with files, where each transaction in the layer is defined as a file operation. A D7A file defines different properties associated with every data element such as storage class, permissions, etc. Most of the transactions possible with a regular file such as read, write, append and delete are available with D7A files, with the ALP providing an interface to access and work with these files. The utilization of a structured data element like a file makes the transaction across DASH7 devices seamless and easy. For instance, a sensor can be defined as a file on a DASH7 device which a gateway can easily remotely access using the file name alone, without bothering the underlying complexities of the sensor. In addition to ALP, the application layer defines D7A Action Protocols (D7AActP) which can be used to trigger predefined actions conditionally on file access.

2.2 Wireless Sensor Nodes

The design of the sensor node is of utmost importance to ensure the long-term and reliable operation of the network. The sensor node must consume the lowest possible energy while providing an interface to external sensors such as soil temperature sensor, water content sensor, and weather station. Moreover, it must be reliable, modular, and easily re-configurable in architecture to provide a seamless sensor interface that anyone without much technical know-how can deploy and work with. This is an important aspect of the design considering that the network will be deployed miles away and troubleshooting and reconfiguring visits are costly. Therefore, the major aspects of the sensor node design are:

- low power consumption to enable long-term operation.
- support a variety of sensors with different interfaces such as 1-wire, I2C, SPI, SDI-12 and analog.
- work seamlessly with any sensor. This implies the device should not require reprogramming or reconfiguration to support a different sensor, enabling modular architecture.

The hardware architecture of the sensor nodes is based on the low-power OCTA module. OCTA uses a CMWX1ZZABZ-091 radio modem from Murata which can be programmed either as a DASH7 node or as a LoRaWAN node. The OCTA board further provides GPIOs through a 10-pin connector which can be used to connect external peripherals or extension boards. We use an extension board with onboard sensors and components to enable additional sensors and interfaces. The extension board houses a temperature-humidity sensor, an external watchdog timer, flash memory for data buffering, a configurable power supply ($V_{OUT} = 5 \text{ V}, 3.3 \text{ V}$), an ultra-low power ADC, and an on-the-fly configurable GPIO pins. The external Watchdog Timer (WDT) ensures that the device recovers from any unexpected code execution halt. The configurable power supply allows the device to accommodate external sensors with different voltage requirements. The entire hardware of the node is powered using a 19 A h LiSOCl2 primary cell. The device stays in sleep mode most of the time, consuming around $10\,\mu\text{A}$ and wake-ups either when the sampling timer fires or a downlink message is received. A picture of the OCTA module and the extension board is shown in Fig. 3.

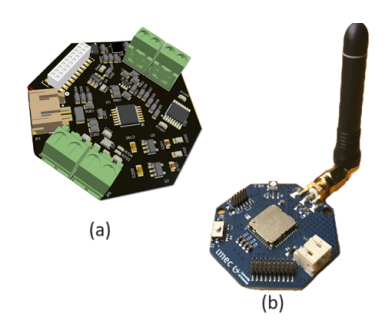


Figure 3: Picture of (a) an extension board with memory, watchdog timer, configurable power supply and IO interfaces (b) OCTA module.

The sensor nodes run open-source DASH7 implementation from SubIoT to enable DASH7 connectivity along with additional application firmware to support and manage sensors and remote access [10]. We configure the stack to operate in PULL mode where the node can be asynchronously accessed and downlink messages can be transmitted down to the node. The application layer of the node is required to perform three primary tasks (i) sample connected sensors at predefined intervals and transmit the data (ii)

provide a seamless interface to sensors and (iii) manage downlink messages and act based on the specific downlink requests. The hardware and software stack of the sensor node is depicted in Fig. 4.

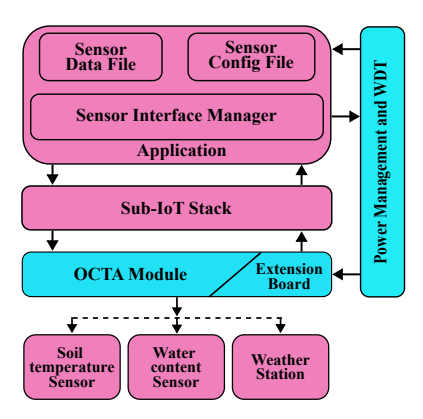


Figure 4: Hardware-software stack of the designed wireless sensor node.

As discussed, DASH7 is a file-based communication protocol, implying that all the transactions happening across the layers are file operations such as file read or write. We exploit this feature to provide remote access and a seamless sensor interface. The application layer defines two main files, one for the sensor data and the other for the sensor configuration. In addition, a Sensor Interface Manager (SIM) provides software re-configurable data lines to the sensors. Any file operation on the sensor data file will trigger a data transmission from the sensor node. This could be a file write action by the SIM after sampling a sensor or a file read command (downlink) from the gateway which triggers spontaneous sensor data transmission.

Listing 1: node configuration file

```
typedef struct {
    union {
        uint8_t raw[NODE_CONFIG_FILE_SIZE];
        struct
        {
            uint8_t sensor_type;
            uint16_t sensor_address;
            uint8_t sensor_action;
            uint8_t sensor_action;
            uint32_t sampling_rate;
            uint32_t rtc_time;
        };
    };
} node_config_file_t;
```

A format of the node configuration file as defined by the application side is shown in listing 1. The file defines <code>sensor_type</code> which specifies the type of sensor connected which could be either a soil temperature, soil water content or a weather station. The <code>sensor_address</code> specifies the address of the device on the corresponding data bus (1-Wire or SDI-12). Every write to the <code>node_config</code> causes an interface reload on the application side. On reload, the SIM checks for the <code>dvice_type</code> and loads the corresponding device

driver for the configured sensor. This is achieved by providing software drivers for the 1-Wire and SDI-12 interfaces, allowing the sensor node to configure the GPIO without requiring any hardware changes. The sampling_time refers to the sensor sampling as well as transmission interval in seconds. The parameter sensor action refers to different actions possible with the sensor, such as triggering a measurement, calibration, power reset, etc. For instance, writing a value 0xAA on this field will cause the SIM to trigger a new measurement with the sensor and transmit the results immediately. The time of the Real-Time Clock (RTC) on the device can be configured via the rtc time field which accepts time in Unix Timestamp format. When updating a single field in the file, the whole file doesn't need to be written, instead, the particular field can be updated by using an offset with the read or write action. For instance, a write action with offset = 3 will only update the sensor action field. A sequence diagram showing different file actions and transactions is shown in Fig. 5.

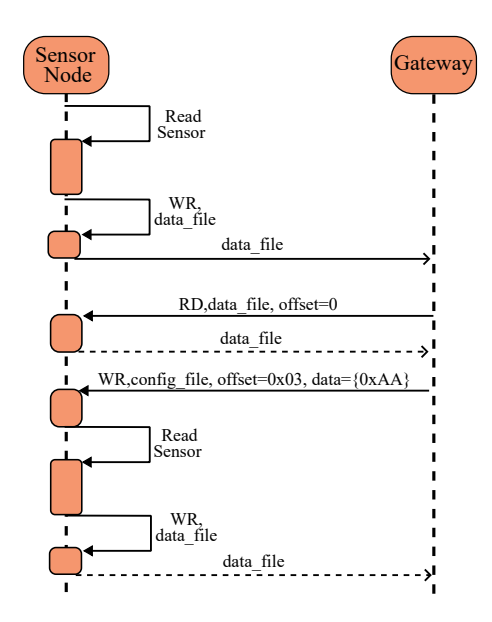


Figure 5: Sequence diagram representation of uplink and downlink communication between the sensor node and gate-

2.3 Gateway

A wireless gateway is required to collect the data from all the sensor nodes deployed and route it to a backend or central service where the data can be stored and accessed as required. Therefore, the gateway should have two network interfaces, one communicating with the low-power sensor nodes and the other for routing data over an internet connection to the backend. Consequently, the power consumption of the gateways is significantly higher than the sensor nodes, making the selection of network interface and power supply crucial. The deployment sites were located in remote points with no direct access to wired internet connectivity or power supply. Since there was NB-IoT connectivity available, the only option available was to rely on available GPRS connectivity for internet access. However, GPRS connectivity demands a very high power consumption which cannot be supplied with primary cells.

Therefore, we set up a solar power station with 100 W solar panel and a 100 A h battery. In addition, to withstand the extremely low weather conditions where temperature can go down well below 0 $^{\circ}$ C, a battery with self-heating was used. This ensures that the battery lifetime is not impacted by low-temperature conditions.

A picture of the hardware of the gateway is shown in Fig. 6. Similar to the sensor node, the gateway runs a Sub-IoT stack configured in DASH7 gateway mode. However, the gateway does not implement the application layer, instead, the packets are handled at the backend. A cellular modem from Quectel is used to provide GPRS connectivity.



Figure 6: A Picture of the assembled PCB of the GPRS-DASH7 gateway board.

2.4 Network Architecture

The deployment sites are scattered over a wide area with each site divided by hilly terrain. Moreover, none of the sites have direct access to power or internet connectivity. Therefore, we decided to deploy an independent star network at each location as shown in Fig. 7. This implies each site needs a gateway and power which we provide using GPRS connectivity and solar power stations. The gateway connects to the backend which runs the database and visualization framework as depicted in Fig. 7. MQTT is employed to enable data transfer between the gateway and the backend. We use Influxdb to store the collected data and Grafana to visualize the data.

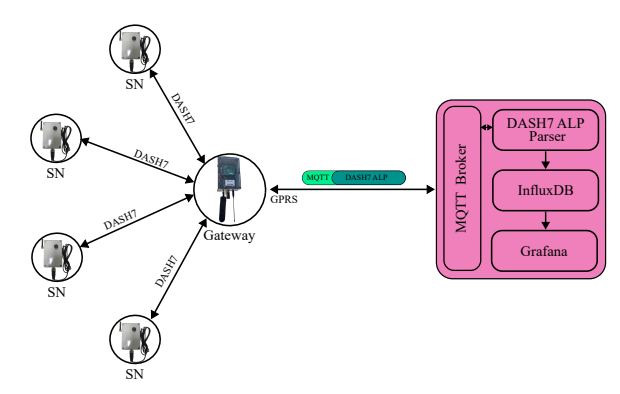


Figure 7: A diagrammatic representation of the LPWAN and the backend framework for data storage and visualization.

Enabling Remote Access: As stated earlier, the DASH7 gateway does not parse the application layer packets. Instead, it forwards

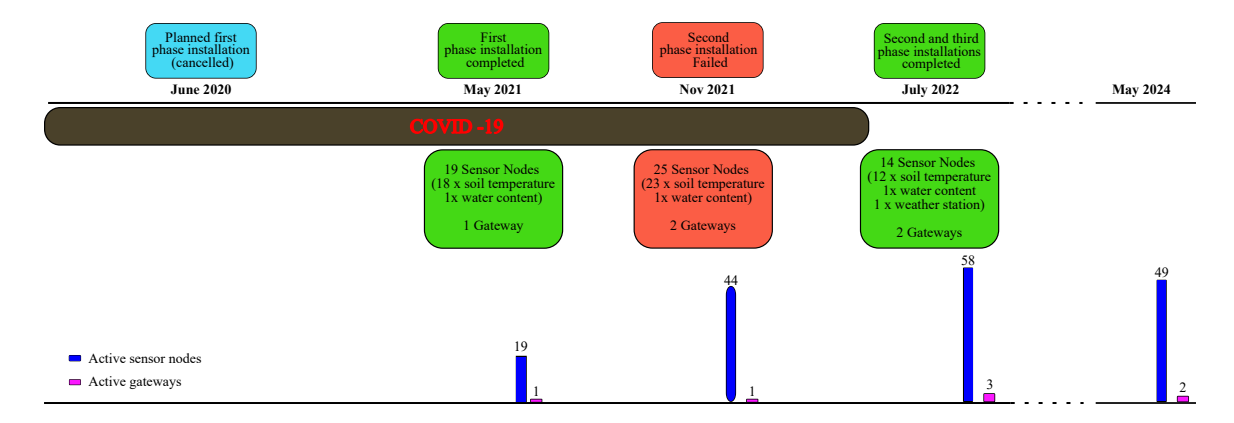


Figure 8: Deployment timeline.

the raw packets to the backend. The ALP of the gateway stack is implemented at the backend in Python using the pyd7a package available from Sub-IoT [9]. pyd7a allows splitting the DASH7 stack between a low-end and a high-end device; for instance, a low-power microcontroller and a remote virtual machine. This brings another advantage that the backend can talk to the remote sensor nodes in a similar way as the gateway would do; i.e., using file names and node IDs. Therefore, a sensor node in the field can be directly accessed from the backend without bothering about the gateway. The communication between the application layer and the network layer happens over MQTT, wrapping DASH7 packets in MQTT.

3 DEPLOYMENT

The deployment of LPWAN and sensor nodes at the three sites happened in different phases as depicted in Fig. 8. The deployment was planned to be carried out in different phases with each phase covering deploying LPWAN and GN 1-3, GN 4-5 and GO respectively. The incremental deployment was also motivated by the hilly and harsh terrain of the sites which were not easy to access and complete with minimal resources in one go. The FN site was excluded from deployment as other experiments were running at the site. The first deployment, i.e., at the GN 1-3 was planned to carry out in June 2020, covering the first 3 plots and 18 transects. The deployment would therefore involve 18 soil temperature sensors, one water content sensor at GN 3F and a gateway. Considering the immediate requirement of data for other researchers in the team, it was decided to use primary cells-powered sensors and incrementally upgrade them to thermal energy-powered devices. Unfortunately, all the plans went in vain, with the massive outbreak of COVID-19 and subsequent lockdowns and travel restrictions. Eventually, the first phase of deployment was carried out in May 2021.

After the successful deployment of the network at GN 1-3, we tried to combine both the GN 4-5 and GO in another attempt in November 2021. This phase intended to deploy 12 soil temperature sensors in GN 4-5 and 24 in GO, a water content sensor in each site and a weather station. Nonetheless, the deployment failed due to adverse weather conditions and reduced daylight hours in the winter. Specifically, moving heavy solar panels, batteries and associated infrastructure for the solar power station became difficult

to carry out and hence the deployment was eventually abandoned. However, the sensor nodes already deployed on the field were left as it is. The gateways and solar power station deployment were subsequently carried out in July/Aug 2022. After the successful third phase, we had total 58 sensor nodes and 3 gateways active in the field. Out of which, 18 nodes and one gateway have been operational since May 2021 and the remaining till July 2022. Data collected from the experiment so far are publicly accessible. In June 2023, sensor nodes from GO were moved to a new experiment site close to GN 4-5 and they communicate with the GN 4-5 gateway. In addition, six of the GN 1-3 have stopped sending data. As of June 2024, we have a total of 49 sensor nodes active.

4 FEASIBILITY OF GEOTHERMAL ENERGY HARVESTING

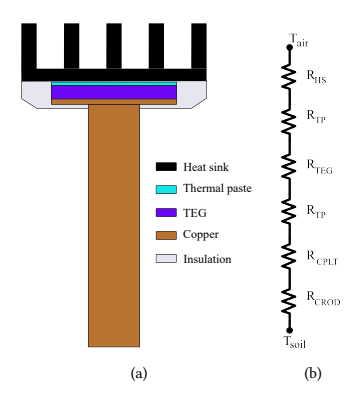


Figure 9: Geothermal energy harvester (a) sketch (b) equivalent thermal resistance diagram.

Considering the soil at the Forhot site is geothermally warmed, a Thermolectric Generator (TEG) may be employed to scavenge energy by exposing it to the temperature gradient caused by the soil and the air. We try to analyse how much energy can be harnessed from the transects using a generic thermal resistance model of an energy harvester. The architecture of the energy harvester which exposes one side of the TEG to the soil through a heat conductor

such as a copper rod and dissipates this heat to the ambient air through a convective heat dissipator such as a heat sink is as shown in Fig. 9a. This is the simplest and most commonly used architecture for scavenging energy from soil-air temperature differences [3, 6]. Referring to the equivalent thermal resistance diagram shown in Fig. 9b, the temperature difference across the TEG can be written as.

$$\Delta T = (T_{soil} - T_{air}) \frac{R_{TEG}}{R_{HS} + R_{TEG} + 2R_{TP} + R_{CPLT} + R_{CROD}} \quad (1)$$

Where T_{soil} is the temperature of the soil, T_{air} is the temperature of the air, R_{TEG} is the thermal resistance of the TEG, R_{HS} is the thermal resistance of the heat sink, R_{CROD} is the thermal resistance of the copper rod, R_{CPLT} is the thermal resistance of the copper plate between copper rod and the TEG and R_{TP} is the thermal resistance of the thermal paste.

Once the temperature difference across the TEG is known, its matched load power can be calculated as [1],

$$P_{TEG} = \frac{(\alpha \Delta T)^2}{4R_{TEG}} \tag{2}$$

Where α is the Seebeck coefficient of the TEG and R_{TEG} is the electrical resistance of the TEG. Therefore, if we know the values of thermal resistances and the properties of the TEG, an approximate estimation of the power generated by the harvester in Fig. 9a can be calculated. We use this method to estimate the one-year power output of the harvester for all the transects in the plot GN 3. We use the TEG TG12-6 with a dimension of 40 mm x 40 mm, thermal resistance 1.58 K/W and Seebeck coefficient 40 mV/K [4, 6]. A heat sink with a thermal resistance of 0.65 K/W with natural convection is used. It must be noted that the thermal resistance of the heat sink varies with wind speed and for more accurate readings wind speed may be considered. The copper rod has a diameter for 2 cm and a length of 10 cm giving a thermal resistance of 0.82 K/W. A thermal paste with a negligible thermal resistance of 0.005 $K - in^2W$ is assumed. The copper plate has a dimension of 40 mm x 40 mm 0.8 mm, creating a thermal resistance of 0.0013 K/W. The copper plate is directly attached to the copper rod and provides a resting base for the hot side of the TEG.

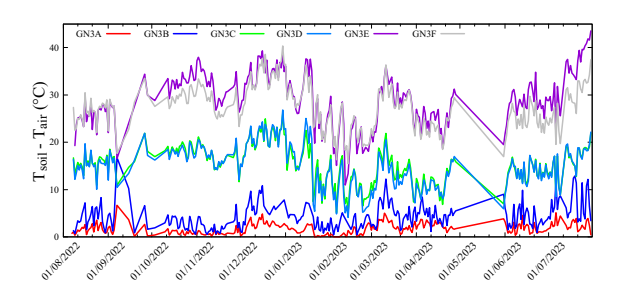


Figure 10: Daily average of the temperature difference between air and soil for each transect in GN 3 plot.

A plot of the daily average of temperature differences recorded for each transect in GN 3 plot is shown in Fig. 10. As stated earlier, the transects are warmed to different levels which is also visible from the graph. Consequently, the average yearly temperature difference recorded are 1.78 °C, 4.31 °C, 15.29 °C, 14.99 °C, 29.0 °C and

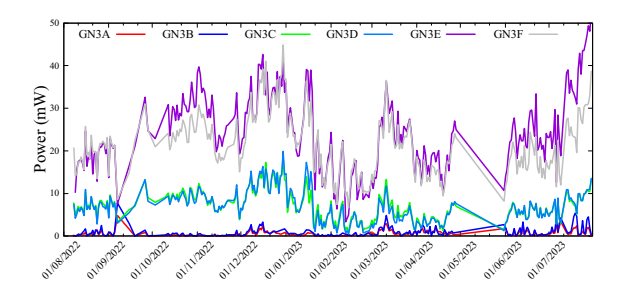


Figure 11: Daily average of the generated power estimated each transect in GN 3 plot.

27.3 °C for the transects A, B, C, D, E and F respectively. It must also be noted that we used a temperature sensor with passive ventilation for air temperature measurements, causing the temperature to be slightly impacted by solar radiation. Using the temperature data and eq. 1 and eq. 2, we estimated the thermal energy which is plotted in Fig. 11. Aligned with the temperature difference values, the yearly average power produced is, 0.572 mW, 0.867 mW, 7.05 mW, 6.93 mW, 24.27 mW and 21.3 mW for the A, B, C, D, E and F transects respectively. Therefore, while the four transects C, D, E and F generate sufficient energy, amount of energy harnessed from A and B sites are extremely low. This was one of the primary reasons for running the initial phases of deployments with primary cell-powered devices. However, our subsequent research has generated energy-aware hardware and software that can run even at transects A and B without relying on primary cells.

5 CONCLUSION

We have discussed the design, deployment and maintenance of low-power wireless sensor networks for monitoring and sensing at the geothermally heated ForHot sites in Iceland. The networks have been running for around three years and successfully collecting data. The low-power DASH7 network provides real-time data and downlink communication with little energy overhead. Moreover, the soil and air temperature data provides initial insights into the feasibility of harnessing energy from the geothermally warm soils. While all the sensors are powered with primary cells, we are currently in the process of testing and deploying soil-air thermal energy-powered devices to ensure long-term unattended operation.

REFERENCES

- Diana Enescu. 2019. Thermoelectric energy harvesting: basic principles and applications. Green energy advances 1 (2019), 38.
- [2] ForHot. [n. d.]. Natural soil warming in natural grasslands and a Sitka spruce forest in Iceland. https://forhot.is/ Online; accessed: 2024-06-07.
- [3] Natsuki Ikeda, Ryo Shigeta, Junichiro Shiomi, and Yoshihiro Kawahara. 2020. Soil-monitoring sensor powered by temperature difference between air and shallow underground soil. Proceedings of the ACM on Interactive, Mobile, Wearable and Ubiquitous Technologies 4, 1 (2020), 1–22. https://doi.org/10.1145/3380995
- [4] Marlow Industries. [n. d.]. Single-Stage Thermoelectric Generator. https://www.digikey.be/nl/htmldatasheets/production/1958589/0/0/1/tg12-6-datasheet Online; accessed: 2024-01-01.
- [5] Riccardo Marini, Konstantin Mikhaylov, Gianni Pasolini, and Chiara Buratti. 2022. Low-Power Wide-Area Networks: Comparison of LoRaWAN and NB-IoT Performance. *IEEE Internet of Things Journal* 9, 21 (2022), 21051–21063. https://doi.org/10.1109/JIOT.2022.3176394
- [6] Priyesh Pappinisseri Puluckul and Maarten Weyn. 2024. Harvesting Energy from Soil-Air Temperature Differences for Batteryless IoT Devices: A Case Study. IEEE Access 12 (2024), 85306–85323. https://doi.org/10.1109/ACCESS.2024.3414652

- [7] Jörn PW Scharlemann, Edmund VJ Tanner, Roland Hiederer, and Valerie Kapos. 2014. Global soil carbon: understanding and managing the largest terrestrial carbon pool. *Carbon management* 5, 1 (2014), 81–91.
- [8] Bjarni D Sigurdsson, Niki IW Leblans, Steven Dauwe, Elin Gudmundsdottir, Per Gundersen, Gunnhildur E Gunnarsdottir, Martin Holmstrup, Krassimira Ilieva-Makulec, Thomas Katterer, Brynd-S Marteinsdottir, et al. 2016. Geothermal ecosystems as natural climate change experiments: The ForHot research site in Iceland as a case study. Icelandic agricultural sciences.-Reykjavik, Akureyri 29 (2016), 53-71.
- [9] Sub-IoT. [n. d.]. DASH7 Python Support. Retrieved June 7, 2024 from https://github.com/Sub-IoT/pyd7a
- [10] SubIoT. [n. d.]. Implementation of the DASH 7 Alliance protocol. Retrieved June 7, 2024 from https://sub-iot.github.io/Sub-IoT-Stack
- [11] Maarten Weyn, Glenn Ergeerts, Rafael Berkvens, Bartosz Wojciechowski, and Yordan Tabakov. 2015. DASH7 alliance protocol 1.0: Low-power, mid-range sensor and actuator communication. In 2015 IEEE Conference on Standards for Communications and Networking (CSCN). IEEE, 54–59. https://doi.org/10.1109/ CSCN.2015.7390420